ARTICLE

# Imaging and Tuning Molecular Levels at the Surface of a Gated Graphene Device

Alexander Riss,[†,▽,⊗,*] Sebastian Wickenburg,[†,‡,⊗] Liang Z. Tan,[†,‡] Hsin-Zon Tsai,[†] Youngkyou Kim,[†,§] Jiong Lu,[†,∞,¥] Aaron J. Bradley,[†] Miguel M. Ugeda,[†] Kacey L. Meaker,[†] Kenji Watanabe,[∥] Takashi Taniguchi,[∥] Alex Zettl,[†,‡] Felix R. Fischer,[‡,⊥,#,*] Steven G. Louie,[†,‡] and Michael F. Crommie[†,‡,#,*]

[†]Department of Physics, [§]Department of Chemical and Biomolecular Engineering, [⊥]Department of Chemistry, University of California, Berkeley, California 94720, United States, [‡]Materials Sciences Division, Lawrence Berkeley National Laboratory, Berkeley, California 94720, United States, [∥]Advanced Materials Laboratory, National Institute for Materials Science, 1-1 Namiki, Tsukuba, 305-0044, Japan, [#]Kavli Energy NanoSciences Institute, University of California and the Lawrence Berkeley National Laboratory, Berkeley, California 94720, United States, [∞]Graphene Research Centre, National University of Singapore, 6 Science Drive 2, Singapore 117546, Singapore, and [¥]Department of Chemistry, National University of Singapore, 3 Science Drive 3, Singapore 117543, Singapore. [⊗]A.R. and S.W. contributed equally. [▽]Present address: Institute of Applied Physics, Vienna University of Technology, Wiedner Hauptstrasse 8-10, 1040 Vienna, Austria.

**ABSTRACT** Gate-controlled tuning of the charge carrier density in graphene devices provides new opportunities to control the behavior of molecular adsorbates. We have used scanning tunneling microscopy (STM) and spectroscopy (STS) to show how the vibronic electronic levels of 1,3,5-tris(2,2-dicyanovinyl)benzene molecules adsorbed onto a graphene/BN/$SiO_2$ device can be tuned *via* application of a backgate voltage. The molecules are observed to electronically decouple from the graphene layer, giving rise to well-resolved vibronic states in d*I*/d*V* spectroscopy at the single-molecule level. Density functional theory (DFT) and many-body spectral function calculations show that these states arise from molecular orbitals coupled strongly to carbon−hydrogen rocking modes. Application of a back-gate voltage allows switching between different electronic states of the molecules for fixed sample bias.

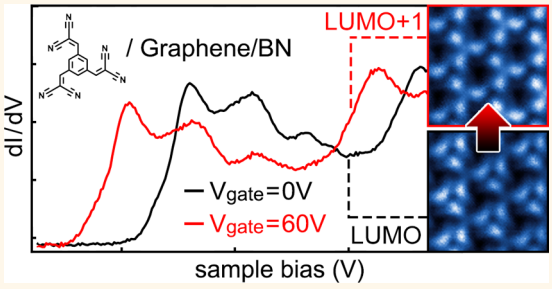


**KEYWORDS:** graphene · organic molecules · vibronic levels · scanning tunneling microscopy · scanning tunneling spectroscopy · density functional theory · GW self-energy

Combining organic molecules with graphene creates new opportunities for fabricating hybrid devices with tailored properties. Previous experiments have shown that electronic,[1−18] magnetic,[6,19,20] and optical[21−23] characteristics as well as chemical reactivity[22,24,25] of graphene devices can be tuned through molecular adsorption. Such measurements have been performed primarily using electrical conductivity and optical spectroscopy techniques. These measurements, however, do not directly yield local microscopic information regarding the hybrid graphene/molecule interface. Additional electronic structure information on molecule/graphene systems in nongated configurations has been provided by STM[14,15,20,26−33] and photoemission spectroscopy[7,13,14,18,29,34,35] experiments, including measurement of the energy location of molecular orbitals. Such measurements, however, have so far precluded the hybrid molecule/graphene electronic structure from being electrostatically tuned through the use of a back-gate, and molecular vibronic properties in these systems remain poorly understood.[32]

Here we describe a single-molecule-resolved STM study of a molecular monolayer adsorbed onto a back-gated graphene device (Figure 1a) that allows both characterization and gate-induced modification of molecular electronic properties. 1,3,5-Tris-(2,2-dicyanovinyl)benzene (CVB) molecules were adsorbed onto a graphene device in ultrahigh vacuum (UHV) and studied *via* STM spectroscopy at cryogenic temperatures. Hybridized electronic levels of individual CVB molecules on graphene were imaged, and the electronic states were observed to exhibit unexpectedly strong vibronic satellites. The hybridized vibronic

* Address correspondence to riss@iap.tuwien.ac.at, ffischer@berkeley.edu, crommie@berkeley.edu.

Received for review March 14, 2014 and accepted April 18, 2014.

**Published online April 18, 2014**
**10.1021/nn501459v**

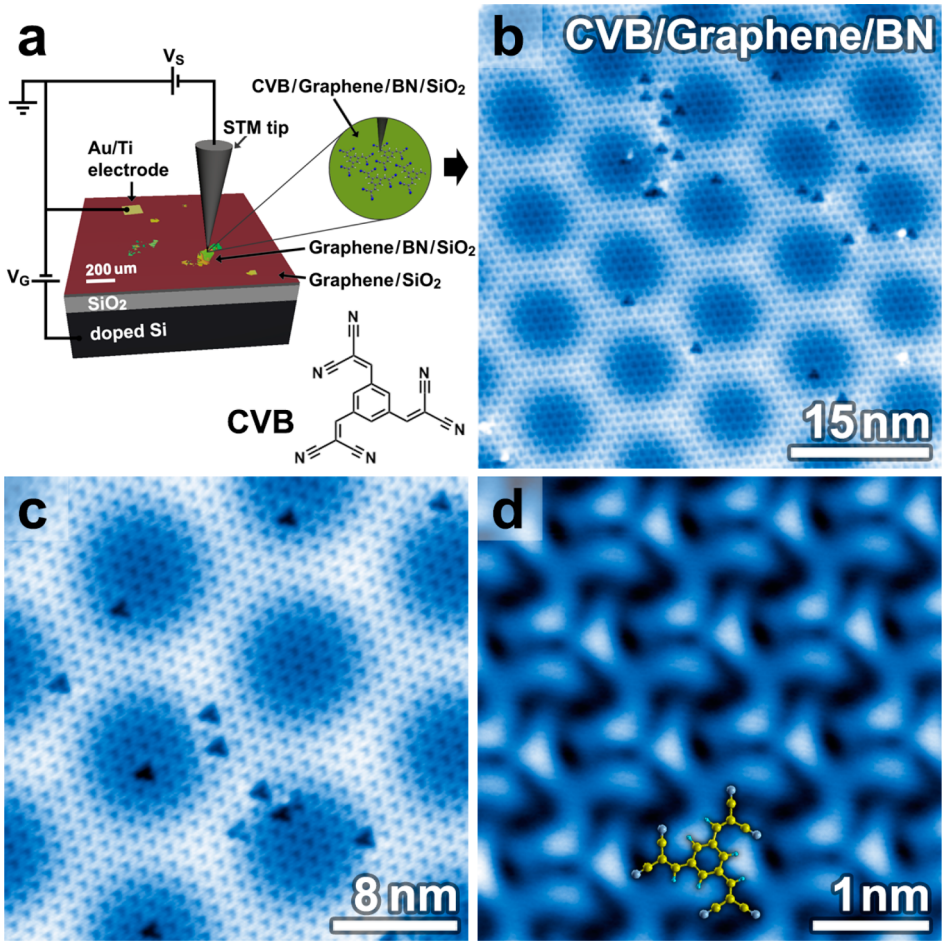


**Figure 1. CVB molecules on a graphene/BN/$SiO_2$ FET device. (a) Sketch of the back-gated graphene device used in these STM/STS measurements, as well as a model of the CVB molecule. (b–d) STM images of a monolayer of CVB molecules on graphene/BN show the hexagonal lattice of the CVB molecules at different zoom values ($V_S$ = 2.0 V, $I_t$ = 10 pA, $T$ = 4 K). Isolated vacancies are observed in (b) and (c).**

electronic structure of the CVB molecules rigidly shifted in energy as a voltage was applied to the device back-gate, thus allowing the electronic local density of states (LDOS) at fixed sample bias to be switched between different molecular orbitals. Identification of the experimentally observed molecular orbitals was facilitated *via* density functional theory (DFT) based spectral function simulations which accurately reproduce the orbital structure imaged by STM. These simulations also allow identification of the vibronic satellites through calculation of the CVB electron–phonon coupling. Although CVB molecules exhibit a broad spectrum of vibrational modes, only C–H rocking modes of the CVB molecules having an energy close to 200 meV are seen to contribute significantly to the molecule/graphene electron–phonon coupling. The energy of these modes is in good agreement with the energy spacing of vibronic satellites observed experimentally for CVB on graphene.

## RESULTS AND DISCUSSION

Parts b–d of Figure 1 show STM images of a monolayer-high self-assembled island of CVB molecules on graphene/BN. The Moiré pattern arising from interaction between the graphene lattice and the underlying BN lattice is clearly visible (Figure 1b,c) even though the graphene is covered with a layer of molecules. The molecules form a hexagonal lattice with a lattice constant of $a$ = 1.13 ± 0.01 nm, and isolated defects having triangular shape can be observed. The close-up STM image in Figure 1d shows a spiral-like electronic LDOS that is associated with the molecules (the opposite chirality was also observed in different islands). The presence of single-molecule vacancies (Figures 1b,c) allows us to assign the location of CVB molecules in the film.

d*I*/d*V* spectra were measured while holding the STM tip above the CVB monolayer. The spectra were essentially featureless over the range $-0.5\ V < V_S < +1.6\ V$, but for $V_S > 1.6$ V clear resonance features were observed (Figure 2a). For $V_S < -0.5$ V the CVB molecules tended to jump to the STM tip, and so reproducible STM spectra at sample voltages lower than −0.5 V could not be obtained. The Dirac point of the underlying graphene substrate could be seen when the tip height was lowered by 4 Å relative to

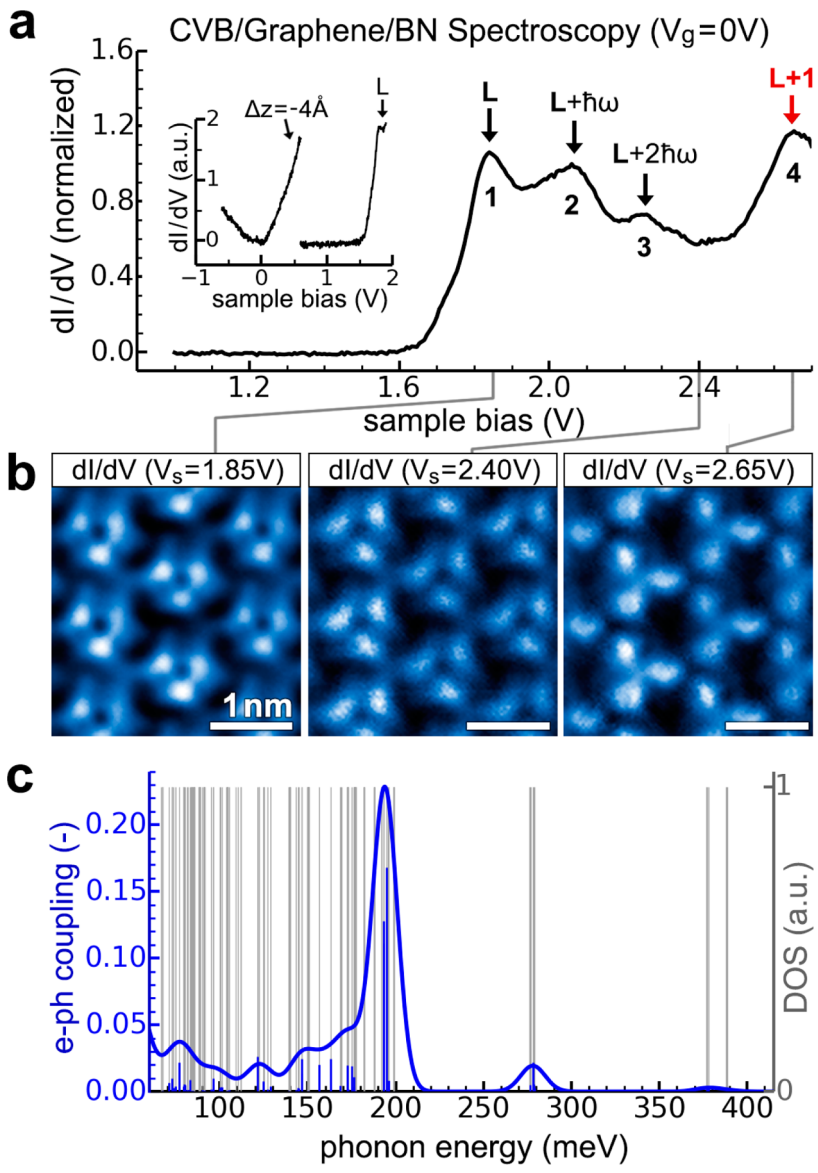


**Figure 2. STM spectroscopy of CVB/graphene/BN reveals vibronic response. (a) d*I*/d*V* spectrum measured with STM tip held above a monolayer of CVB molecules on a graphene/BN FET device ($V_G = 0$). Spectrum is featureless over the range $-0.5$ V < $V_S$ < 1.6 V but shows four clear molecule-induced resonances (marked 1−4) in the range 1.6 V < $V_S$ < 2.8 V (junction set-point parameters $V_S = 2.7$ V, $I_t = 160$ pA; the spectrum is normalized by its value at 2.6 V). Inset shows a section of the d*I*/d*V* spectrum over the range $-0.6$ V < $V_S$ < 0.6 V where the tip has been lowered by 4 Å relative to other spectra (junction set-point parameters: $V_S = 0.6$ V, $I_t = 40$ pA; tip is closer because $V_S$ now lies in the HOMO−LUMO gap). Here the Dirac point can be observed at $V_S \approx 0$ V ($V_G = 0$ V). Inset also shows onset of peak 1 (0.6 V < $V_S$ < 1.9 V) for typical junction set-point parameters: $V_S = 1.9$ V, $I_t = 40$ pA. Peaks 1 and 4 are interpreted as LUMO and LUMO+1, respectively, while peaks 2 and 3 are interpreted as vibronic satellites of the LUMO (see text). (b) Experimental d*I*/d*V* maps obtained at voltages $V_S = 1.85$, 2.4, and 2.65 V ($V_G = 0$ V). d*I*/d*V* maps taken in the range 1.85 V < $V_S$ < 2.4 V probe the local density of states (LDOS) of peaks 1−3 and look very similar. The d*I*/d*V* map taken at $V_S = 2.65$ V probes peak 4 and yields a LDOS pattern that is different from the pattern observed for peaks 1−3. (c) Calculated density of states (DOS) of vibrational modes of CVB molecules on graphene (gray lines), as well as the electron−phonon coupling strength between the CVB vibrational modes and the CVB LUMO state (vertical blue lines). The blue curve shows the calculated electron−phonon coupling broadened with a Gaussian function of width 16 meV.**

the typical d*I*/d*V* measurement tip-height (Figure 2a inset), but this usually led to CVB molecules jumping to the STM tip. The empty state spectrum for larger tip heights, however, was quite stable up to nearly 3 V, as seen in the spectrum of Figure 2a (this spectrum was reproduced with numerous different tips and samples). Four pronounced peaks can be seen in the spectrum, labeled 1−4. A statistical analysis of our spectra (using Gaussian fits to the peaks) yields the following energy locations for the four peaks (where $E = |e|V_S$): $E_1 = 1.86 \pm 0.02$ eV, $E_2 = 2.06 \pm 0.02$ eV, $E_3 = 2.28 \pm 0.02$ eV, and $E_4 = 2.68 \pm 0.03$ eV. The energy differences between peaks 1−2 and peaks 2−3 are quite similar, whereas the energy difference between peaks 3−4 is twice as big: $E_2 - E_1 = 0.20 \pm 0.03$ eV, $E_3 - E_2 = 0.22 \pm 0.03$ eV, and $E_4 - E_3 = 0.40 \pm 0.04$ eV. d*I*/d*V* maps taken

at sample biases covering the range of the first three peaks (1.85 V < $V_S$ < 2.4 V) show no significant differences in the spatial distribution of the electronic LDOS (Figure 2b, first two panels). However, the d*I*/d*V* map obtained at the energy of the fourth peak ($V_S$ = 2.65 V) shows a significantly different spatial distribution of the electronic LDOS (Figure 2b, third panel).

One of the unique aspects of this study is that we were able to perform STM spectroscopy and imaging while modifying the hybridized molecule/graphene electronic doping using an electrostatic back-gate. Figure 3a shows d*I*/d*V* spectra taken on a CVB monolayer island at two different back-gate voltages ($V_G$). The black trace shows the spectrum acquired at $V_G$ = 0 V while the red trace shows the spectrum taken at a gate voltage of $V_G$ = 60 V. The red trace is rigidly shifted by ~0.2 V toward lower sample bias but does not exhibit any other significant changes in its features. We see a similar gate−dependent shift in the Dirac point energy *via* STM spectroscopy for these graphene devices without molecular layers,[36] corresponding to a change in the carrier concentration from $n = 4 \times 10^{10}$ cm$^{-2}$ ($V_G$ = 0 V) to $n = 4 \times 10^{12}$ cm$^{-2}$ ($V_G$ = 60 V). We next acquired d*I*/d*V* maps at a fixed sample bias of $V_S$ = 2.4 V, but for different gate voltages $V_G$. The d*I*/d*V* map acquired at $V_G$ = 0 V (Figure 3b) shows the same features as observed at biases corresponding to peaks 1−3 (Figure 2b, first two panels), but the d*I*/d*V* map acquired at $V_G$ = 60 V (Figure 3c) exhibits a significantly different LDOS that is similar to what was observed previously for peak 4 (Figure 2b, third panel). The LDOS at this fixed energy with respect to $E_F$ can thus be toggled between two different molecular orbitals *via* application of a positive gate voltage (this orbital switching is reversible and has no hysteresis).

We are able to understand our gate-dependent local electronic structure measurements of the hybrid CVB/graphene system through the use of first-principles simulations. The main questions we wish to answer here concern the origin and behavior of spectroscopic peaks 1−4 (Figures 2 and 3). To do this, we performed density functional theory (DFT) calculations of the combined CVB/graphene system using an exchange-correlation functional which combines the PBE functional together with a semi-empirical dispersion correction to take into account van der Waals interactions between the molecules and graphene.[37,38] After correcting for electron−electron[39−41] and electron−phonon interactions[42,43] in the electron self-energy (see the Supporting Information), we obtained a HOMO−LUMO energy gap of 6.3 eV and a (LUMO)−(LUMO+1) energy gap of 0.8 eV. Although our experimental energy range does not allow us to experimentally verify the predicted HOMO−LUMO gap, we note that the theoretical (LUMO)−(LUMO+1) energy almost perfectly matches the experimental energy difference between peaks 1 and 4 ($\Delta E_{14}$ = 0.82 ± 0.04 eV).

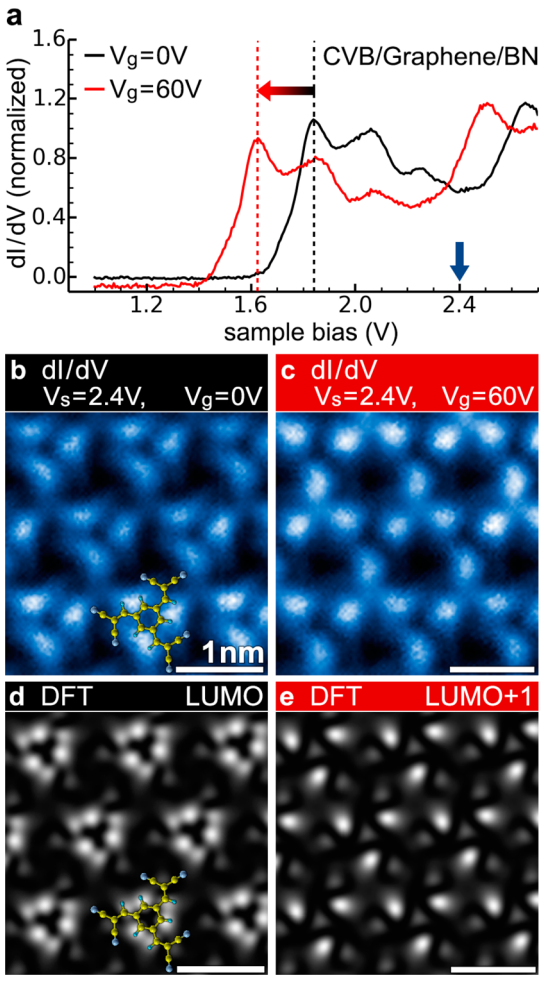


**Figure 3. Gate-induced shift of the electronic levels of CVB molecules on a graphene/BN FET device: (a) d*I*/d*V* spectra of CVB/graphene/BN at two different gate voltages: $V_G$ = 0 V (black trace) and $V_G$ = 60 V (red trace). Increasing the gate voltage to $V_G$ = 60 V causes a rigid downward shift of the molecular electronic resonances by 0.2 eV, consistent with the gate-induced shift seen in the Dirac point for graphene/BN devices without adsorbed molecules (spectra are normalized by their respective values at $V_S$ = 2.6 V). (b) Experimental d*I*/d*V* map obtained with $V_S$ = 2.4 V and $V_G$ = 0 V. (c) Same as (b) except that $V_G$ = 60 V. (d) Theoretical local density of states map of the CVB/graphene LUMO state calculated using DFT. (e) Same as (d) except for LUMO+1 state. These maps show that changing the device gate voltage allows the STM to access different molecular orbitals for a fixed sample bias.**

This suggests that peak 1 is the CVB/graphene LUMO and that peak 4 is the LUMO+1 state. To further test this hypothesis we calculated the theoretical LDOS of the LUMO and LUMO+1 states and compared it to the experimental d*I*/d*V* maps measured at the energies of peaks 1 and 4. The theoretical LDOS of these different states (Figure 3d,e) is in good agreement with the experimental LDOS maps (first panel and third panel in Figure 2b), thus providing additional evidence that peaks 1 and 4 correspond to the system's LUMO and LUMO+1 states (this procedure also allowed us to confirm the molecular orientation shown in Figures 1 and 3).

An important remaining question is the origin of peaks 2 and 3, which do not appear in the calculated DOS obtained *via* DFT. These peaks clearly have some relation to the LUMO state, since their experimental d*I*/d*V* maps are essentially identical to the d*I*/d*V* map for peak 1 (Figure 2b), and they strongly resemble the theoretical LDOS map that was calculated for the LUMO state (Figure 3d). We believe that these additional peaks (2 and 3) arise due to the existence of vibronic modes of the CVB molecule on graphene. Such modes reflect coupling between the electronic and vibrational states of a molecule and result in new features in the electron spectral function. Vibronic modes have been seen previously in STM spectroscopy of molecules that are decoupled from a metallic substrate[44−46] (single-particle vibronic modes are quenched by direct molecular coupling to a metallic electrode[44,46]). The spacing between vibronic satellites corresponds to the quantum of vibrational energy ($\hbar\omega$) for the molecular vibrational state that is entangled with the electronic orbital. Vibronic states do not appear in DFT calculations of electronic levels because the Born−Oppenheimer assumption prevents mixing of electronic states with vibrational modes.

To verify this picture, we calculated the theoretical vibrational modes for CVB molecules on graphene as well as the electron−phonon coupling that exists between the molecular LUMO state and each vibrational mode. While the molecular vibrations span a wide energy range, we seek to understand whether strong electron−phonon coupling exists for any modes having energy similar to the energy difference between peaks 1 and 2 (0.2 eV), as well as between peaks 2 and 3 (0.22 eV). The gray lines in Figure 2c show the theoretical vibrational modes of CVB on graphene, calculated within the framework of DFT perturbation theory. As expected, they span a wide energy range, up to 400 meV. The calculated electron−phonon coupling strength between these modes and the CVB LUMO state is shown by the bold blue trace in Figure 2c (see eq SI-6 in the Supporting Information for a detailed definition of this quantity). The electron−phonon coupling shows a strong peak at the modes near 200 meV, in good agreement with the experimental value of $\Delta E_{12}$ and $\Delta E_{23}$ which have an average value of 210 meV. From this calculation we are able to determine that the modes with high electron−phonon coupling at 200 meV mainly involve C−H rocking vibrations (which have representations $A_1'$, $E_1'$, and $E_2'$ of the $C_{3h}$ point group) suggesting that this particular type of vibration is the origin of the vibronic satellites observed experimentally as peaks 2 and 3 (a detailed calculation of electronic LDOS within the first order cumulant approximation for the electron−phonon coupling is shown in the Supporting Information).

This vibronic interpretation of the d*I*/d*V* spectrum helps to explain the gate-dependent orbital switching observed in d*I*/d*V* maps obtained at a fixed tip−sample bias of $V_S = 2.4$ V. Here a gate voltage of $V_G = 0$ V yields a d*I*/d*V* map reflecting the LUMO density (Figures 3b,d) while a gate voltage of $V_G = 60$ V yields a d*I*/d*V* map reflecting the LUMO+1 density (Figures 3c,e). Within a vibronic picture the fixed tip−sample bias at $V_G = 0$ V probes the peak 3 resonance which is a vibronic LUMO satellite, whereas gating at $V_G = 60$ V shifts the tunnel current to the peak 4 resonance which reflects the LUMO+1 state. Electrostatic gating thus allows a fixed tip−sample bias to switch between imaging the LUMO and LUMO+1 orbitals.

## CONCLUSIONS

In conclusion, we have shown that CVB molecules adsorbed onto a graphene/BN device self-assemble into a hexagonal lattice and develop vibronic peaks that correspond to coupling of electrons to the $A_1'$, $E_1'$, and $E_2'$ rocking modes of the CVB carbon−hydrogen bonds. The fact that vibronic peaks can be so readily resolved in the molecule/graphene spectra shown here suggests that substrate-induced lifetime broadening is weak on graphene due to electronic decoupling of adsorbed molecules.[44,46] Gating the hybrid molecule/graphene device allows electronic switching between two different molecular states (LUMO and LUMO+1) for a fixed tip−sample bias voltage. Extensions of this approach can be envisioned that might allow exploration of gate-controlled changes in molecular functionality for hybrid graphene devices at the single-molecule level.

## METHODS

We used back-gated graphene/BN/$SiO_2$ devices[47−49] similar to the one schematically depicted in Figure 1a. The graphene sample was grown by the CVD method described in ref 49. Hexagonal boron nitride flakes were exfoliated onto heavily doped silicon wafers coated by a 285 nm thermal oxide. The graphene was transferred on top of the BN/$SiO_2$[49] using a polydimethylsiloxane (PDMS) stamp, and electrical contact was made by depositing Ti (10 nm thick)/Au (30 nm-thick) electrodes using a stencil mask technique.

1,3,5-Tris(2,2-dicyanovinyl)benzene (CVB) was synthesized through a Knoevenagel condensation of benzene-1,3,5-tricarboxaldehyde and malononitrile.[51,52] The molecules were evaporated from a Knudsen cell onto the graphene device in UHV while the device was held at $T = 5$ K. The device was then briefly annealed at room temperature before being cooled back to 4 K. CVB was chosen for this experiment due to its extended $\pi$-system and the high electron affinity of its dicyanovinyl groups.

STM/STS was performed using an Omicron LT STM at $T = 4$ K. STM differential conductance (d*I*/d*V*) was measured in constant-height mode (both for point spectroscopy and for spatial maps) by lock-in detection of the a.c. tunnel current generated by a 6 mV rms 316 Hz signal added to the sample bias.

DFT calculations were performed using an exchange-correlation functional that combines the PBE functional together with a semi-empirical dispersion correction to take into account van der Waals interaction between the molecules and graphene.[37,38] We used a supercell containing one CVB molecule and 42 graphene atoms, with a lattice constant of 1.13 nm. The combined CVB and graphene system was allowed to relax in these simulations to its most stable configuration. Frequencies of vibrational modes and electron−phonon matrix elements were calculated in the framework of density functional perturbation theory (DFPT)[42] using the QUANTUM ESPRESSO package.[43] We performed GW[39,40] corrections employing the BerkeleyGW package[41] to account for electron−electron correlations not captured in DFT. The molecular orbital energies were further corrected for electron−phonon interactions using the first-order cumulant approximation (see the Supporting Information).

*Conflict of Interest:* The authors declare no competing financial interest.

*Supporting Information Available:* Calculation of molecular electronic LDOS in the presence of strong electron−phonon coupling utilizing the cumulant expansion. This material is available free of charge *via* the Internet at http://pubs.acs.org.

*Acknowledgment.* This research was supported by the Nanomachine program at the Lawrence Berkeley National Laboratory funded by the Director, Office of Science, Office of Basic Energy Sciences of the US Department of Energy under Contract No. DE-AC02-05CH11231 (STM and nc-AFM instrumentation development, AFM operation, GW calculations and surface renormalization analysis), and by the National Science Foundation awards DMR-1235361 (image analysis), DMR10-1006184 (DFT calculations), and EEC-0832819 (molecule/graphene device preparation). A.R. acknowledges fellowship support by the Austrian Science Fund (FWF): J3026-N16. J.L. acknowledges fellowship support from the Singapore grant "Novel 2D materials with tailored properties: beyond graphene" (R-144-000-295-281). S.G.L. acknowledges support from a Simons Foundation Fellowship in Theoretical Physics. A.J.B. was supported by the Department of Defense (DoD) through the National Defense Science & Engineering Graduate Fellowship (NDSEG) Program. We acknowledge the assistance of the XSEDE computational cluster resource provided by NICS (Kraken), supported by the National Science Foundation. Graphene growth characterization at the LBNL Molecular Foundry was supported by the Office of Science, Office of Basic Energy Sciences, of the US Department of Energy under Contract No. DE-AC02-05CH11231.

*Note Added after ASAP Publication:* This paper was published on May 2, 2014. Affiliations were added, the Acknowledgment section and the Supporting Information was modified. The revised version was reposted on May 7, 2014.

## REFERENCES AND NOTES

1. Schedin, F.; Geim, A. K.; Morozov, S. V.; Hill, E. W.; Blake, P.; Katsnelson, M. I.; Novoselov, K. S. Detection of Individual Gas Molecules Adsorbed on Graphene. *Nat. Mater.* **2007**, *6*, 652–655.
2. Sojoudi, H.; Baltazar, J.; Tolbert, L. M.; Henderson, C. L.; Graham, S. Creating Graphene P−N Junctions Using Self-Assembled Monolayers. *ACS Appl. Mater. Interfaces* **2012**, *4*, 4781–4786.
3. Peimyoo, N.; Li, J.; Shang, J.; Shen, X.; Qiu, C.; Xie, L.; Huang, W.; Yu, T. Photocontrolled Molecular Structural Transition and Doping in Graphene. *ACS Nano* **2012**, *6*, 8878–8886.
4. Lee, B.; Chen, Y.; Duerr, F.; Mastrogiovanni, D.; Garfunkel, E.; Andrei, E. Y.; Podzorov, V. Modification of Electronic Properties of Graphene with Self-Assembled Monolayers. *Nano Lett.* **2010**, *10*, 2427–2432.
5. Kim, M.; Safron, N. S.; Huang, C.; Arnold, M. S.; Gopalan, P. Light-Driven Reversible Modulation of Doping in Graphene. *Nano Lett.* **2012**, *12*, 182–187.
6. Georgakilas, V.; Otyepka, M.; Bourlinos, A. B.; Chandra, V.; Kim, N.; Kemp, K. C.; Hobza, P.; Zboril, R.; Kim, K. S. Functionalization of Graphene: Covalent and Non-Covalent Approaches, Derivatives and Applications. *Chem. Rev.* **2012**, *112*, 6156–6214.
7. Coletti, C.; Riedl, C.; Lee, D. S.; Krauss, B.; Patthey, L.; von Klitzing, K.; Smet, J. H.; Starke, U. Charge Neutrality and Band-Gap Tuning of Epitaxial Graphene on SiC by Molecular Doping. *Phys. Rev. B* **2010**, *81*, 235401.
8. Zhang, Z.; Huang, H.; Yang, X.; Zang, L. Tailoring Electronic Properties of Graphene by $\pi-\pi$ Stacking with Aromatic Molecules. *J. Phys. Chem. Lett.* **2011**, *2*, 2897–2905.
9. Wei, P.; Liu, N.; Lee, H. R.; Adijanto, E.; Ci, L.; Naab, B. D.; Zhong, J. Q.; Park, J.; Chen, W.; Cui, Y.; *et al.* Tuning the Dirac Point in CVD-Grown Graphene through Solution Processed N-Type Doping with 2-(2-Methoxyphenyl)-1,3-dimethyl-2,3-dihydro-1H-benzoimidazole. *Nano Lett.* **2013**, *13*, 1890–1897.
10. Wang, X.; Xu, J.-B.; Xie, W.; Du, J. Quantitative Analysis of Graphene Doping by Organic Molecular Charge Transfer. *J. Phys. Chem. C* **2011**, *115*, 7596–7602.
11. Mao, H. Y.; Lu, Y. H.; Lin, J. D.; Zhong, S.; Wee, A. T. S.; Chen, W. Manipulating the Electronic and Chemical Properties of Graphene via Molecular Functionalization. *Prog. Surf. Sci.* **2013**, *88*, 132–159.
12. Jobst, J.; Waldmann, D.; Speck, F.; Hirner, R.; Maude, D. K.; Seyller, T.; Weber, H. B. Transport Properties of High-Quality Epitaxial Graphene on 6H-SiC(0001). *Solid State Commun.* **2011**, *151*, 1061–1064.
13. Tadich, A.; Edmonds, M. T.; Ley, L.; Fromm, F.; Smets, Y.; Mazej, Z.; Riley, J.; Pakes, C. I.; Seyller, T.; Wanke, M. Tuning the Charge Carriers in Epitaxial Graphene on SiC(0001) from Electron to Hole via Molecular Doping with C60F48. *Appl. Phys. Lett.* **2013**, *102*, 241601.
14. Choi, J.; Lee, H.; Kim, K.; Kim, B.; Kim, S. Chemical Doping of Epitaxial Graphene by Organic Free Radicals. *J. Phys. Chem. Lett.* **2010**, *1*, 505–509.
15. Yang, H.; Mayne, A. J.; Comtet, G.; Dujardin, G.; Kuk, Y.; Sonnet, Ph.; Stauffer, L.; Nagarajan, S. Gourdon, A. STM Imaging, Spectroscopy and Manipulation of a Self-Assembled PTCDI Monolayer on Epitaxial Graphene. *Phys. Chem. Chem. Phys.* **2013**, *15*, 4939–4946.
16. Loh, K. P.; Bao, Q.; Ang, P. K.; Yang, J. The Chemistry of Graphene. *J. Mater. Chem.* **2010**, *20*, 2277.
17. Yan, L.; Zheng, Y. B.; Zhao, F.; Li, S.; Gao, X.; Xu, B.; Weiss, P. S.; Zhao, Y. Chemistry and Physics of a Single Atomic Layer: Strategies and Challenges for Functionalization of Graphene and Graphene-Based Materials. *Chem. Soc. Rev.* **2012**, *41*, 97–114.
18. Chen, W.; Chen, S.; Qi, D. C.; Gao, X. Y.; Wee, A. T. S. Surface Transfer P-Type Doping of Epitaxial Graphene. *J. Am. Chem. Soc.* **2007**, *129*, 10418–10422.
19. Nair, R. R.; Tsai, I.-L.; Sepioni, M.; Lehtinen, O.; Keinonen, J.; Krasheninnikov, A. V.; Castro Neto, A. H.; Katsnelson, M. I.; Geim, A. K.; Grigorieva, I. V. Dual Origin of Defect Magnetism in Graphene and Its Reversible Switching by Molecular Doping. *Nat. Commun.* **2013**, *4*, 2010.
20. Garnica, M.; Stradi, D.; Barja, S.; Calleja, F.; Díaz, C.; Alcamí, M.; Martín, N.; Vázquez de Parga, A. L.; Martín, F.; Miranda, R. Long-Range Magnetic Order in a Purely Organic 2D Layer Adsorbed on Epitaxial Graphene. *Nat. Phys.* **2013**, *9*, 368–374.
21. Ling, X.; Wu, J.; Xu, W.; Zhang, J. Probing the Effect of Molecular Orientation on the Intensity of Chemical Enhancement Using Graphene-Enhanced Raman Spectroscopy. *Small* **2012**, *8*, 1365–1372.
22. Liu, J.; Tang, J.; Gooding, J. J. Strategies for Chemical Modification of Graphene and Applications of Chemically Modified Graphene. *J. Mater. Chem.* **2012**, *22*, 12435–12452.
23. Zhao, X.; Yan, X.-Q.; Ma, Q.; Yao, J.; Zhang, X.-L.; Liu, Z.-B.; Tian, J.-G. Nonlinear Optical and Optical Limiting Properties of Graphene Hybrids Covalently Functionalized by Phthalocyanine. *Chem. Phys. Lett.* **2013**, *577*, 62–67.
24. Xue, T.; Jiang, S.; Qu, Y.; Su, Q.; Cheng, R.; Dubin, S.; Chiu, C.-Y.; Kaner, R.; Huang, Y.; Duan, X. Graphene-Supported Hemin as a Highly Active Biomimetic Oxidation Catalyst. *Angew. Chem., Int. Ed.* **2012**, *51*, 3822–3825.
25. Wang, Q. H.; Jin, Z.; Kim, K. K.; Hilmer, A. J.; Paulus, G. L. C.; Shih, C.-J.; Ham, M.-H.; Sanchez-Yamagishi, J. D.; Watanabe, K.;

Taniguchi, T.; *et al.* Understanding and Controlling the Substrate Effect on Graphene Electron-Transfer Chemistry via Reactivity Imprint Lithography. *Nat. Chem.* **2012**, *4*, 724–732.
26. Xiao, K.; Deng, W.; Keum, J. K.; Yoon, M.; Vlassiouk, I. V.; Clark, K. W.; Li, A.-P.; Kravchenko, I. I.; Gu, G.; Payzant, E. A.; *et al.* Surface-Induced Orientation Control of CuPc Molecules for the Epitaxial Growth of Highly Ordered Organic Crystals on Graphene. *J. Am. Chem. Soc.* **2013**, *135*, 3680–3687.
27. Wang, Q. H.; Hersam, M. C. Room-Temperature Molecular-Resolution Characterization of Self-Assembled Organic Monolayers on Epitaxial Graphene. *Nat. Chem.* **2009**, *1*, 206–211.
28. Järvinen, P.; Hämäläinen, S. K.; Banerjee, K.; Häkkinen, P.; Ijäs, M.; Harju, A.; Liljeroth, P. Molecular Self-Assembly on Graphene on $SiO_2$ and h-BN Substrates. *Nano Lett.* **2013**, *13*, 3199–3204.
29. Huang, H.; Chen, S.; Gao, X.; Chen, W.; Wee, A. T. S. Structural and Electronic Properties of PTCDA Thin Films on Epitaxial Graphene. *ACS Nano* **2009**, *3*, 3431–3436.
30. Lauffer, P.; Emtsev, K. V.; Graupner, R.; Seyller, T.; Ley, L. Molecular and Electronic Structure of PTCDA on Bilayer Graphene on SiC(0001) Studied with Scanning Tunneling Microscopy. *Phys. Status Solidi* **2008**, *245*, 2064–2067.
31. Hossain, M. Z.; Walsh, M. A.; Hersam, M. C. Scanning Tunneling Microscopy, Spectroscopy, and Nanolithography of Epitaxial Graphene Chemically Modified with Aryl Moieties. *J. Am. Chem. Soc.* **2010**, *132*, 15399–15403.
32. Wang, Y.-L.; Ren, J.; Song, C.-L.; Jiang, Y.-P.; Wang, L.-L.; He, K.; Chen, X.; Jia, J.-F.; Meng, S.; Kaxiras, E.; *et al.* Selective Adsorption and Electronic Interaction of $F_{16}CuPc$ on Epitaxial Graphene. *Phys. Rev. B* **2010**, *82*, 245420.
33. Cho, J.; Smerdon, J.; Gao, L.; Özgün, S.; Guest, J. R.; Guisinger, N. P. Structural and Electronic Decoupling of $C_{60}$ from Epitaxial Graphene on SiC. *Nano Lett.* **2012**, *12*, 3018–3024.
34. Ying Mao, H.; Wang, R.; Wang, Y.; Chao Niu, T.; Qiang Zhong, J.; Yang Huang, M.; Chen, Qi. D.; Ping Loh, K.; Thye Shen Wee, A.; Chen, W. Chemical Vapor Deposition Graphene as Structural Template to Control Interfacial Molecular Orientation of Chloroaluminium Phthalocyanine. *Appl. Phys. Lett.* **2011**, *99*, 093301.
35. Zhou, S. Y.; Siegel, D. A.; Fedorov, A. V.; Lanzara, A. Metal to Insulator Transition in Epitaxial Graphene Induced by Molecular Doping. *Phys. Rev. Lett.* **2008**, *101*, 086402.
36. Brar, V. W.; Wickenburg, S.; Panlasigui, M.; Park, C.-H.; Wehling, T. O.; Zhang, Y.; Decker, R.; Girit, Ç.; Balatsky, A. V.; Louie, S. G.; *et al.* Observation of Carrier-Density-Dependent Many-Body Effects in Graphene via Tunneling Spectroscopy. *Phys. Rev. Lett.* **2010**, *104*, 036805.
37. Grimme, S. Semiempirical GGA-Type Density Functional Constructed with a Long-Range Dispersion Correction. *J. Comput. Chem.* **2006**, *27*, 1787–1799.
38. Barone, V.; Casarin, M.; Forrer, D.; Pavone, M.; Sambi, M.; Vittadini, A. Role and Effective Treatment of Dispersive Forces in Materials: Polyethylene and Graphite Crystals as Test Cases. *J. Comput. Chem.* **2009**, *30*, 934–939.
39. Hybertsen, M.; Louie, S. First-Principles Theory of Quasiparticles: Calculation of Band Gaps in Semiconductors and Insulators. *Phys. Rev. Lett.* **1985**, *55*, 1418–1421.
40. Hybertsen, M. S.; Louie, S. G. Electron Correlation in Semiconductors and Insulators: Band Gaps and Quasiparticle Energies. *Phys. Rev. B* **1986**, *34*, 5390–5413.
41. Deslippe, J.; Samsonidze, G.; Strubbe, D. A.; Jain, M.; Cohen, M. L.; Louie, S. G. BerkeleyGW: A Massively Parallel Computer Package for the Calculation of the Quasiparticle and Optical Properties of Materials and Nanostructures. *Comput. Phys. Commun.* **2012**, *183*, 1269–1289.
42. Baroni, S.; de Gironcoli, S.; Dal Corso, A.; Giannozzi, P. Phonons and Related Crystal Properties from Density-Functional Perturbation Theory. *Rev. Mod. Phys.* **2001**, *73*, 515–562.
43. Giannozzi, P.; Baroni, S.; Bonini, N.; Calandra, M.; Car, R.; Cavazzoni, C.; Ceresoli, D.; Chiarotti, G. L.; Cococcioni, M.; Dabo, I.; *et al.* QUANTUM ESPRESSO: A Modular and Open-Source Software Project for Quantum Simulations of Materials. *J. Phys.: Condens. Matter* **2009**, *21*, 395502.
44. Qiu, X. H.; Nazin, G. V.; Ho, W. Vibronic States in Single Molecule Electron Transport. *Phys. Rev. Lett.* **2004**, *92*, 206102.
45. Pavliček, N.; Swart, I.; Niedenführ, J.; Meyer, G.; Repp, J. Symmetry Dependence of Vibration-Assisted Tunneling. *Phys. Rev. Lett.* **2013**, *110*, 136101.
46. Wang, S.; Wang, W.; Hong, Y.; Tang, B. Z.; Lin, N. Vibronic State Assisted Resonant Transport in Molecules Strongly Anchored at an Electrode. *Phys. Rev. B* **2011**, *83*, 115431.
47. Novoselov, K. S.; Geim, A. K.; Morozov, S. V.; Jiang, D.; Zhang, Y.; Dubonos, S. V.; Grigorieva, I. V.; Firsov, A. A. Electric Field Effect in Atomically Thin Carbon Films. *Science* **2004**, *306*, 666–669.
48. Zhang, Y.; Brar, V. W.; Wang, F.; Girit, C.; Yayon, Y.; Panlasigui, M.; Zettl, A.; Crommie, M. F. Giant Phonon-Induced Conductance in Scanning Tunnelling Spectroscopy of Gate-Tunable Graphene. *Nat. Phys.* **2008**, *4*, 627–630.
49. Decker, R.; Wang, Y.; Brar, V. W.; Regan, W.; Tsai, H.; Wu, Q.; Gannett, W.; Zettl, A.; Crommie, M. F. Local Electronic Properties of Graphene on a BN Substrate via Scanning Tunneling Microscopy. *Nano Lett.* **2011**, *11*, 2291–2295.
50. Li, X.; Cai, W.; An, J.; Kim, S.; Nah, J.; Yang, D.; Piner, R.; Velamakanni, A.; Jung, I.; Tutuc, E.; *et al.* Large-Area Synthesis of High-Quality and Uniform Graphene Films on Copper Foils. *Science* **2009**, *324*, 1312–1314.
51. Naito, K.; Sakurai, M.; Egusa, S. Molecular Design, Syntheses, and Physical Properties of Nonpolymeric Amorphous Dyes for Electron Transport. *J. Phys. Chem. A* **1997**, *101*, 2350–2357.
52. Andresen, T. L.; Krebs, F. C.; Larsen, M.; Thorup, N.; Lönnberg, H.; Yan, S.-P.; Wang, G.-L.; Yao, X.-K.; Wang, H.-G.; Tuchagues, J.-P.; *et al.* Crystal Structure of Three Compounds Related to Triphenylene and Tetracyanoquinodimethane. *Acta Chem. Scand.* **1999**, *53*, 410–416.